UC Riverside

UC Riverside Electronic Theses and Dissertations

Title

Evolution of Chemical and Optical Properties of Secondary Organic Aerosols Generated from Nighttime Oxidation of Unsaturated Heterocyclic Compounds

Permalink

https://escholarship.org/uc/item/2kg0135v

Author

Raeofy, Nilofar

Publication Date

2021

Peer reviewed|Thesis/dissertation

UNIVERSITY OF CALIFORNIA
RIVERSIDE

Evolution of Chemical and Optical Properties of Secondary Organic Aerosols Generated
from Nighttime Oxidation of Unsaturated Heterocyclic Compounds

A Thesis submitted in partial satisfaction
of the requirements for the degree of

Master of Science

in

Environmental Sciences

by

Nilofar R. Raeofy

June 2021

Thesis Committee:
        Dr. Roya Bahreini, Chairperson
        Dr. Ying-Hsuan Lin
        Dr. Haofei Zhang

The Thesis of Nilofar R. Raeofy is approved:

_____

_____

_____
                                    Committee Chairperson

University of California, Riverside

ACKNOWLEDGMENTS

In the first place, I would like to thank my advisor Dr. Roya Bahreini for allowing me to join her research group and for imparting her knowledge and expertise in all possible ways during my master's program period. The completion of this dissertation would not have been possible without her outstanding support, mentorship, and more importantly patience in addressing all the questions I had. Working under her supervision has been one of the most enjoyable experiences I have had in my life.

I would also like to thank Dr. Ying-Hsuan Lin and Dr. Haofei Zhang for serving on my committee and for their directions, comments, and feedbacks when we had meetings for the progress of my project.

To my lab mates, Yumeng, Hossein, and Kunpeng thank you for all the research experiences you've shared with me and helping me through my questions. Thank you for your friendship and company.

Last but not least, many thanks to my friends and family for their continuous support. If it wasn't for your encouragement and support, I wouldn't have become the person I am today.

ABSTRACT OF THE THESIS

Evolution of Chemical and Optical Properties of Secondary Organic Aerosols Generated
from Nighttime Oxidation of Unsaturated Heterocyclic Compounds

by

Nilofar R. Raeofy

Master of Science, Graduate Program in Environmental Sciences
University of California, Riverside, June 2021
Dr. Roya Bahreini, Chairperson

Studies have shown that the secondary organic aerosols (SOA), generated from
the oxidation reactions of organic compounds, can produce light-absorbing species
referred to as secondary brown carbon (BrC).[1] BrC is a significant contributor to climate
radiative forcing and atmospheric warming, however, chemical composition and optical
properties of BrC aerosols remain poorly understood. Biomass burning (BB) has been
recognized as the major source of primary and secondary BrC aerosols in the
atmosphere.[2-4] The nighttime chemistry in BB plumes ca enhance the formation of BrC
in the atmosphere.[5,6] Heterocyclic compounds are emitted in large quantities from BB
smoke and can act as possible precursors for BrC formation.

In this work, we investigated the optical properties and chemical evolution of BrC
formed during the nighttime NO_3-initiated oxidation of furan, furfural, pyrrole, 1-
methylpyrrole, and thiophene in laboratory chamber studies. Pyrrole oxidation led to
formation of the most absorbing BrC, followed by furan- and furfural- derived SOA.

Thiophene and 1-methylpyrrole oxidation produced only slightly absorbing SOA. Trends in signatures of different SOA functional groups are investigated to explain the observed differences in the measured optical properties: single scattering albedo (SSA), mass absorption coefficient (MAC), and refractive index (RI) of SOA.

TABLE OF CONTENTS

LIST OF FIGURES

LIST OF TABLES

CHAPTER I: INTRODUCTIONS

1.1 Atmospheric Aerosols

Atmospheric aerosols, consisting of solid or liquid particles suspended in air, play a major role in the atmosphere. The Fifth Assessment Report by the Intergovernmental Panel on Climate Chang (IPCC) (AR5) estimated a global mean direct radiative (RF) forcing of -0.35 (-0.85 to +0.15) W m^{-2} for aerosols due to aerosol-light interaction with RF of -0.09 (–0.16 to –0.03) and –0.03 (–0.27 to +0.20) for primary and secondary organic aerosols (generated from fossil fuel and biofuel combustions), respectively.[7]

Aerosols can scatter or absorb incoming solar radiation and significantly influence the Earth's radiative balance; they affect the distribution and abundance of trace gases, and influence cloud formation.[8,9] Atmospheric aerosols also have important impacts on human health, causing damaging effects on cardiovascular and respiratory systems.[10,11] Atmospheric aerosols can be formed from natural and anthropogenic sources. They can be emitted directly from different sources such as fossil fuels combustions, biomass burning, and wind-driven processes (e.g. sea salt, soil, and mineral dust). They can be formed in the atmosphere through gas-particle conversion processes (e.g. nucleation, condensation, and heterogenous reactions).[8]

1.2 Secondary Organic Aerosols (SOA)

Organic aerosols (OA) comprise a large fraction (20-90%) of submicron aerosols in the atmosphere. [12–14] Organic aerosols that are directly emitted into the atmosphere are referred to as primary organic aerosols (POA). Volatile/ intermediate volatility/ semi-

1

volatile organic compounds (VOCs, IVOCs, and SVOCs, respectively) can undergo oxidation in the gas phase to yield products with sufficiently low vapor pressures that can condense to the particle phase, generating secondary organic aerosols (SOA). It is estimated that SOA accounts for 70-90% of OA mass.[8] Light-absorbing aerosols such as black carbon (BC), mineral dust, and brown carbon (BrC) have been shown to result in positive radiative forcing.[15,16] BrC and BC can be emitted directly from biomass burning and fossil fuel combustion. BrC can also be produced secondarily as SOA in the atmosphere.[1,9] While BC absorbs light in a wide range from ultraviolet (UV) to infrared, BrC light absorption is strongly wavelength-dependent, increases toward the shorter wavelengths of visible (400-700 nm) and into near ultraviolet and ultraviolet region (200-400 nm).[17–19]

Identification of BrC chromophores is highly crucial for the determination of BrC optical properties and their direct radiative effects.[20,21] The organic fraction of aerosols consists of hundreds of different species making it challenging to identify chromophores that are responsible for light absorption. Several studies have suggested that nitro-aromatic species in aerosols are a potentially important contributor to near-UV light absorption and they account for 4% of light absorption by BrC.[20,22] Additionally, condensation reactions involving carbonyls and ammonium salts, amines, and amino acids can result in light-absorbing products that could account for at most 10% of the global light absorption by BrC.[23,24] Recently, nitro-containing heterocyclic compounds (e.g. nitropyrrole) have also been found to be an important component of BrC.[5]

1.3 Aerosol Optical Properties

The extent of scattering and absorption of light by aerosols strongly depend on particle's size, shape, morphology, chemical composition, refractive index, and wavelength of the incident light. Single scattering albedo (SSA), mass absorption coefficient (MAC), and complex refractive index (RI) are critical parameters used in models and calculations of aerosol radiative forcing to determine the impacts of light-absorbing aerosols on the Earth's radiative balance.[25–27]

Single scattering albedo denotes the scattering fraction of total extinction while the mass absorption coefficient is expressed as the aerosol absorption per unit organic mass concentration. Also, the imaginary part (k) of the complex RI ($m=n+ik$) can be used to determine the aerosol absorption. In this work, we focus on trends and comparisons of these optical properties in the different systems.

1.4 Biomass Burning Emissions

Biomass burning (BB) including wildfires, agricultural fires, and prescribed fires is a major source of particulate matter (PM), gases such as carbon dioxide (CO_2), nitrogen oxide (NO_x), and a variety of organic compounds with a range of volatilities, e.g., VOCs, IVOCs and SVOCs.[28,29] It is estimated that IVOCs and SVOCs account for 15-37% of BB carbonaceous emissions.[30] With more than 3.9 Tg yr^{-1} emissions, BB aerosols and their subsequent transformations in the atmosphere play a major role in climate and air quality.[31,32] Modeling studies have reported a global radiative forcing of 0.03-0.57 W m^{-2}

attributed to BrC components of BB.[31,33] Studies have shown that BrC in fresh BB organic aerosol contains numerous chromophores with different polarity, volatility, and chemical structure.[34] These BB aerosols, after emission into the atmosphere, can undergo chemical processing, dilution, and coagulation on timescales of seconds to days, which would affect their overall optical properties in the atmosphere.[4,34,35] Unsaturated heterocyclic compounds containing heteroatoms (e.g., N, O, and S) represent a unique family of reactive compounds that are emitted in large quantities during BB events.[5] Hatch et al., estimated emission factors of 5-37% of total emitted carbon for furans (oxygenated aromatic species) during biomass burning events.[29] Moreover, thiophene, sulfur analog to the furan ring, has emission factors similar to that reported for dimethyl sulfide, thus it may be an important source of organosulfur compounds in BB aerosol.[29,36]

Under global warming scenarios, with the increase in global mean temperatures, the number and intensity of wildfires are expected to increase and so does the emission of primary BrC-containing BB aerosols and the precursors for secondary BrC aerosols. Therefore a more comprehensive knowledge of formation pathways and physicochemical nature of these aerosols is essential to provide the input for atmospheric models assessing impacts of wildfires on the radiation budget.[37–39]

1.5 Research Goals

While daytime photochemistry of BB plumes have been studied in a number of laboratories and field studies, much less is known about the nighttime BB emissions oxidative processing.[40,41] Nighttime oxidative processing of BB aerosols are expected to

be dominated by nitrate radicals (NO_3) and O_3.[31,42] In BB emissions, NO_x is emitted in high levels and can readily be oxidized by O_3 to generate NO_3 radicals. Previous studies have shown that major unsaturated heterocyclic compounds can readily react with NO_3, forming absorbing nitroaromatics (RNO_2) or organonitrates (ON, i.e., $RONO_2$) that can partition into particle phase.[5,34]

In this research, the NO_3 oxidation of unsaturated heterocyclic compounds including furfural, furan, thiophene, pyrrole, and 1-methylpyrrole was investigated as probable sources of secondary BrC in laboratory chamber experiments. Seed aerosol and different NO_x/O_3 ratios were used in some experiments to enhance partitioning to particle phase and evaluate kinetics of NO_3 radical formation, respectively. We used both online and offline techniques to evaluate composition and optical properties (e.g., SSA, MAC, and RI at 375 nm) of SOA from different precursors. Chemical evolution of SOA was analyzed to identify potential chromophores.

CHAPTER II: EXPERIMENTAL SETUP

2.1 Chamber Setup and Instrumentation

Experiments were conducted in a 10 m^3 FEP Teflon chamber bag under relative humidity ranging from 0-20 % (TRH-Central, Omega Engineering Inc, temperature and relative humidity probe) at temperatures between 20-25 °C. Figure 2.1 shows the smog chamber setup.
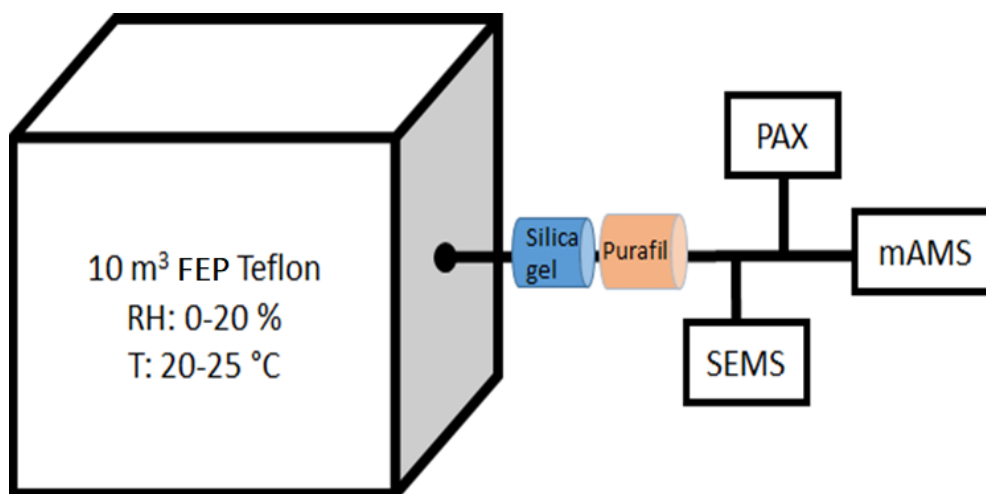
Figure 1: Smog Chamber Set-up

Volatile hydrocarbons used in this study were furan (TCI America, >99%), Thiophene (Alfa Aesar, 99%), pyrrole (TCI America, >99%), furfural (Acros Organics, 99%), and 1-methylpyrrole (TCI America, >99%). O_3 was generated through corona discharge (A2Z Ozone 3GLAB) and injected into the chamber to achieve initial O_3 mixing ratios of ~1500 ppbv. Two different approaches were taken for generating NO_3 in the chamber from the reaction of O_3 with NO_2: 1) Injecting NO_2 (Airgas) followed by the injection of O_3. 2)

Injecting O_3 first followed by the injection of NO (Airgas) to generate NO_2, followed by additional injection of O_3. Two levels of NO_x were aimed for this study with the target initial mixing ratios of ~150 and ~450 ppbv for NO_2. Next, VOC was evaporated into the chamber by flowing N_2 over the liquid in a glass bulb to achieve a mixing ratio of ~200 ppbv. During the seeded experiments, ammonium sulfate (AS) seed particles were introduced into the chamber either by a collision type air-jet atomizer (TSI, Model 3076) or a single-jet atomizer (TSI, Model 9302) by atomizing a 0.02 M solution. The initial number concentration and mode are $11 \times 10^4 - 16.7 \times 10^4$ particles cm^{-3} and $53 - 60$ nm, respectively.

Various instruments sampled air from the chamber through a 30 cm long diffusion dryer filled with silica gel (Sigma-Aldrich) and Purafil (Thermo Scientific). Real-time size-resolved mass distributions and chemical composition of SOA particles were measured using a mini-Aerosol Mass Spectrometer coupled with a compact time-of-flight mass spectrometer (mAMS, Aerodyne Research)[27,43].

A Scanning Electrical Mobility Spectrometer (SEMS, Brechtel Manufacturing Inc.) was used to determine the number concentration and size distribution of SOA particles in the size range of 10-800 nm. Sizing accuracy of the SEMS was determined to be ~$\pm$4% based on calibration with polydisperse polystyrene latex sphere standards (Polysciences, Inc.-Warrington, PA, U.S.A). Counting accuracy of SEMS was determined to be ~$\pm$10%. A Photoacoustic Extinctiometer (PAX, Droplet Measurement Technology) was utilized to measure the scattering and absorption coefficients of SOA particles at 1 Hz at 375 nm ($\beta_{scat,375}$ and $\beta_{abs,375}$). The detection limit defined as 2 times the standard deviation of

scattering and absorption measurements of filtered air averaged to SEMS time (140s) were ~0.8 and ~1 M m^{-1}, respectively. The uncertainties for scattering and absorption measurements have been estimated to be ~ $\pm$ 4.5% and $\pm$ 6%, respectively.[27] Table 1 shows the summary of experimental conditions used in this work.

Table 1: Initial Conditions for Experiments

Hydrocarbon	HC$_o$ (ppb)	Initial [NO$_2$]/[O$_3$]	Seed Aerosol	ρ_{eff} (g/cc)
Furan	200	0.1	No	1.43 $\pm$ 0.01
Furan	200	0.1	Yes	1.42 $\pm$ 0.03
Furan	200	0.3	No	1.37 $\pm$ 0.06
Furfural	200	0.1	No	1.48 $\pm$ 0.04
Furfural	200	0.1	Yes	1.45 $\pm$ 0.05
Furfural	200	0.3	No	1.31 $\pm$ 0.13
Thiophene	200	0.1	No	1.08 $\pm$ 0.01
Thiophene	200	0.1	Yes	1.53 $\pm$ 0.07
Pyrrole	200	0.1	No	
Pyrrole	200	0.1	Yes	
1-methylpyrrole	200	0.1	No	
1-methylpyrrole	200	0.1	Yes	

2.2 Single Scattering Albedo and Mass Absorption Coefficient Calculations

The single scattering albedo (SSA) at 375 nm was calculated by applying $\beta_{scat,375}$ and $\beta_{abs,375}$ in eq 1.

$$SSA_{375} = \frac{\beta_{scat,375}}{\beta_{scat,375}+\beta_{abs,375}} \tag{1}$$

Since SSA depends on particle size and the measurement wavelength, it is useful to explore its dynamic as a function of size parameter (α). α is calculated by the aerosol mobility mode diameter of the size distribution (d_m) measured by SEMS and the radiation wavelength used in PAX ($\lambda = 375$nm), as shown in eq 2.

$$\alpha = \frac{\pi d_m}{\lambda} \tag{2}$$

SSA values are only reported in the non-seeded experiments and the propagated uncertainties for the calculated SSA were determined to be ~5-7% in different experiments. Mass absorption coefficient (MAC) is a critical parameter that can be used to characterize the optical properties of light-absorbing particles at a specific wavelength.[44] Here, MAC at λ=375 nm is calculated using $\beta_{abs,375}$ obtained from PAX and the total aerosol organic mass concentration (M_{OA}) as in eq 3.

$$MAC_{org} = \frac{\beta_{abs,375}}{M_{OA}} \tag{3}$$

The mass concentration of organic aerosol (M_{OA}) can be calculated from the SEMS integrated volume concentration (Vol_{SEMS}) and ρ_{eff} in eq. 4. Using the integrated volume concentration from the SEMS minimizes the uncertainties in OA mass concentration calculations related to particles that bounce off of the AMS vaporizer before flash vaporization.

$$M_{OA} = \left(1 - MF_{inorg}\right) \times Vol_{SEMS} \times \rho_{eff} \tag{4}$$

Where MF_{inorg} is the mass fraction of the inorganic components relative to the total measured particle mass concentration. Given that the observed absorption characteristics

is specifically due to the presence of organic components in the aerosol, the volume and mass fractions of organics in aerosols should be determined in each experiment in order to accurately evaluate the optical parameters (i.e., MAC_{org} and RI_{org}). Effective density is determined by a parallel comparison of AMS mass distributions and SEMS volume distributions.[45] AMS mass distribution is measured versus aerodynamic diameter (d_{va}) while SEMS volume distribution is measured versus electrical mobility diameter (d_m). Assuming particle sphericity, ρ_{eff} can be calculated from eq. 5.

$$\rho_{eff} = \frac{d_{va}}{d_m} \rho_0 \tag{5}$$

Where ρ_0 is unit density (1 g cm^{-3}). In our studies, we determined time-dependent effective densities in both seeded and non-seeded experiments.

Organic mass of aerosol is obtained from the sum of the AMS-measured organic species and organic fraction of nitrate, referred to as organonitrates (ON). Studies have shown that the nitrate portion of organic and inorganic nitrates mainly fragments to NO^+ (m/z=30) and NO_2^+ (m/z=46), and it has been observed that the fragmentation pattern (i.e., $\frac{NO^+}{NO_2^+}$ ratio) of ON and inorganic nitrate compounds such as NH_4NO_3 are very different.[46] Fractional contribution of ON to total nitrate signal was calculated by x.[46]

$$x = \frac{(R_{obs} - R_{NH_4NO_3})(1 + R_{ON})}{(R_{ON} - R_{NH_4NO_3})(1 + R_{ON})} \tag{6}$$

Where R_{obs} is the observed $[NO^+]/[NO_2^+]$ in the experiments, $R_{NH_4NO_3}$ is the measured $[NO^+]/[NO_2^+]$ from the AMS ammonium nitrate calibrations (representing the inorganic nitrate contribution to total NO_3^-)[46], and R_{ON} is obtained from $R_{NH_4NO_3} \times 2.75$.[47] Once x

ratio is calculated, following equations are used to calculate the ON and inorganic nitrate mass concentration.

$$M_{ON} = x \times [NO_3^-] \tag{7}$$

$$M_{inorg\_N} = [NO_3^-] - M_{ON} \tag{8}$$

Next, by assuming AMS-measured NH_4^+ to be from inorganic components in the aerosols in both seeded and non-seeded experiments and SO_4^{2-} species to be only present during the seeded experiments, the mass fractions (MF) of inorganic components relative to the total aerosol mass was calculated as follows.

$$MF_{inorg} = \frac{[NO_3^-]_{inorg}+[NH_4^+]+[SO_4^{2-}]}{[Org]+[NO_3^-]+[SO_4^{2-}]+[NH_4^+]} \tag{9}$$

By calculating NH_4^+ needed to fully neutralize the inorganic NO_3^- (obtained from eq. 8) and SO_4^{2-}, we determined that the inorganic compounds in the particle phase were pure HNO_3 (MW= 63 g mol^{-1}, ρ_{NA}= 1.51 g cm^{-3}) in non-seeded experiments and $(NH_4)_2SO_4$ (MW= 132.14 g mol^{-1}, ρ_{AS}= 1.77 g cm^{-3}) in seeded experiments. With the MF_{inorg} determined, the volume fraction of organics can be determined as follows.

$$VF_{org} = 1 - MF_{inorg} \frac{\rho_{eff}}{\rho_{inorg}} \tag{10}$$

2.3 Organosulfate (OS) Compounds in Thiophene Experiments

Chen et al. proposed a method to apportion organic and inorganic components of sulfate species through investigating AMS-measured sulfate fragmentation patterns of organosulfates and inorganic sulfates.[48] Among all the OS fragments produced through fragmentations, SO^+, SO_2^+, SO_3^+, HSO_3^+, and $H_2SO_4^+$ are the main ions and $\sum HSO$ refers

to the sum of all the five ions. Smaller ions like SO^+, SO_2^+, and SO_3^+ produced during OS fragmentations account for most of the $\sum HSO$ signals whereas HSO_3^+ and $H_2SO_4^+$ ions are only produced by AS. The fractions of HSO_3^+ and $H_2SO_4^+$ (f_{HSO_3} and $f_{H_2SO_4}$) ions (eq. 12-13) provide the basis for distinguishing different types of sulfate-containing compounds.

$$\sum HSO = SO^+ + SO_2^+ + SO_3^+ + HSO_3^+ + H_2SO_4^+ \qquad (11)$$

$$f_{HSO_3} = \frac{HSO_3^+}{\sum HSO} \qquad (12)$$

$$f_{H_2SO_4} = \frac{H_2SO_4^+}{\sum HSO} \qquad (13)$$

Figure 2 shows the $f_{H_2SO_4}$ vs f_{HSO_3} obtained from AMS-measured sulfate signals during thiophene oxidation and pure AS sampling experiments. The green triangular point indicates the fragmentation values of OS standards obtained by Chen et al. from their laboratory studies while the red points indicate the range of values observed for pure AS. Presence of OS can be identified since inorganic AS and OS fall into different regions in the plot. During thiophene experiments, the $f_{H_2SO_4}$ vs. f_{HSO_3} values spread over a broad range, making it challenging to accurately attribute those fractions to OS compounds in the aerosol. However, since the $f_{H_2SO_4}$ vs f_{HSO_3} values for thiophene are extended towards the higher values similar to those of pure AS, we suspect most of the sulfate signal in thiophene experiments to be from oxidized sulfur/ inorganic sulfate compounds in the aerosols. Thus, MF_{inorg} for seeded and non-seeded thiophene runs, were calculated using eq. 9.
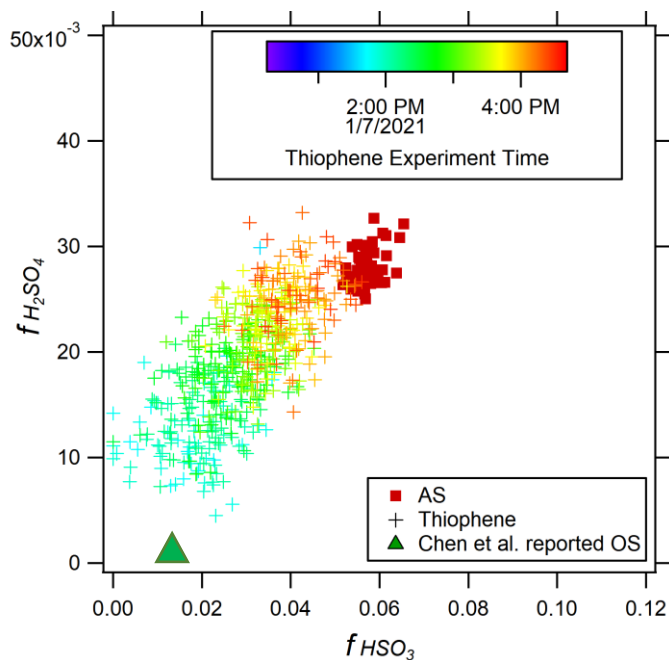
Figure 2: $f_{H_2SO_4}$ vs f_{HSO_3} for Thiophene SOA, AS, and OS

2.4 Refractive Index Calculations

Refractive index (RI) of aerosols is an important parameter which defines the scattering and absorption characteristics of light and is a function of aerosol chemical composition. The complex RI ($m=n+ik$) consists of two components, a real component (n) and the imaginary component (k) that represent scattering and absorption, respectively. Several methods have been used to measure optical properties of aerosols in laboratory studies to derive refractive indices for SOA.[49–51] Those studies have shown that n and k values of RI range from 1.3 to 1.6 and 0.0002 to 0.2, respectively.[9] It has been estimated that k of the OA components of BB ambient aerosols (excluding BC) can reach up to 0.112 at 400 nm.[52] n and k values determine the scattering and absorption efficiencies (Q_{scat} and Q_{abs}) of aerosols when applying Mie theory and for calculating total scattering and

13

absorption coefficients. In order to apply Mie theory, we assumed particles are spherical and homogenous in composition across all sizes. Thus because of particle-size dependence condensation of organics in seeded experiments, the RI values are only reported for the non-seeded experiments. n and k were retrieved by minimizing the difference between the measured and theoretical optical coefficients.[5] Theoretical optical coefficient ($\beta_{scat,theo}$ and $\beta_{abs,theo}$) at 375 nm were calculated for a broad range of n (1-1.8, at 0.01 increments) and k (0-0.05, at 0.001 increments) values, using the measured size distributions at times when the mode change between two consecutive SEMS runs was smaller than 10%. Calculated values of $\beta_{scat,theo}$ and $\beta_{abs,theo}$ were then compared with the measured values of $\beta_{scat,obs}$ and $\beta_{abs,obs}$ by PAX.

$$\beta_{\text{ } scat\text{ } or\text{ } abs,theo} = \sum_{dp,1}^{dp,end} Q_{\text{scat or abs}}(d_i, \lambda, n, k) \times N_i \times \frac{1}{4} \times (\pi \times d_i^2) \tag{17}$$

Where $d_{p,1}$ and $d_{p,end}$ are the smallest and the largest bin diameter, respectively. N_i is the number concentration of aerosols at size d_i. The input n and k values that minimized the merit parameter Δ (eq. 18) were chosen as aerosol's retrieved RI.

$$\Delta = |(\beta_{scat,\,obs} - \beta_{scat,\,theo})| + |(\beta_{abs,\,obs} - \beta_{abs,\,theo})| \tag{18}$$

The retrieved RI includes influence of both organic and inorganic species in the aerosols, thus the following equations were used to calculate the RI of the pure organic species in the aerosols (n_{org} and k_{org})[43].

$$n = n_{inorg} \times VF_{inorg} + n_{org} \times VF_{org} \tag{19}$$

$$k = k_{inorg} \times VF_{inorg} + k_{org} \times VF_{org} \tag{20}$$

Where k_{inorg} and n_{inorg} are the RI values from HNO_3, VF_{org} and VF_{inorg} are the volume fractions of organic and inorganic species, respectively, in the SOA. Note that k_{inorg} is zero for HNO_3.

CHAPTER III: RESULTS AND DISCUSSION

In this project, optical properties and bulk SOA composition are observed under variable NO_x/O_3 conditions in non-seeded experiments where SOA production proceeded via nucleation and seeded experiments where condensation onto pre-existing aerosols was the main pathway toward SOA formation.

3.1 Single Scattering Albedo (SSA)

SSA_{375} values as a function of size parameter and time for all non-seeded experiments are shown in Figure 3. Furfural SOA appeared to be the most absorbing among the five tested precursors, with an average SSA_{375} of 0.7 (higher bound, grey) with pyrrole and furan SOAs coming next with average SSA_{375} values of 0.8 and 0.84, respectively. Thiophene and 1-methylpyrrole SOAs were slightly absorbing with average SSA_{375} values of 0.96 and 0.97, respectively. SSA values for pyrrole and thiophene were similar to those observed by Jiang et al.[5] Since SSA strongly depends on the actual size of the aerosols, once needs to compare its values between experiments and precursors at similar size parameters. For example, furfural and pyrrole SOA have different SSA values as a function of time, but as shown in Figure 3b, one of the furfural SOA has similar SSA values to pyrrole SOA at similar size parameters. In this context, and by projection to higher size parameter values for furan and furfural SOA, results indicate that the most absorbing SOA under low-NO_x conditions was from pyrrole (SSA ~0.8) and the least absorbing SOA was from 1-methylpyrrole and thiophene (SSA ~0.95) while furan and furfural SOA are expected to have intermediate SSA values (~0.85-0.9). SSA as a function of size parameter

16

for furfural and furan under high-NO_x experiments is shown in Figure 4. As observed in Figure 3b, furfural and furan experiments under low-NO_x condition and their repeats showed different SSA values at the same size parameter. Only one experiment was conducted for furfural and furan under high-NO_x condition, thus comparison and evaluation of NO_x effect in these experiments were not possible and more experiments need to be performed.

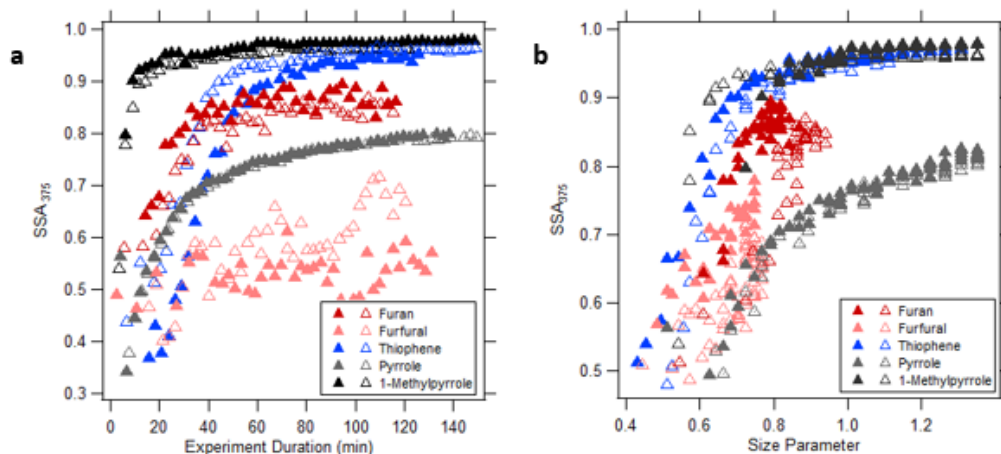Figure 3: SSA a function of a) reaction time b) size parameter at 375 nm for all five precursors under low-NO_x non-seeded conditions. Open and closed markers represent the duplicate runs of the same condition.
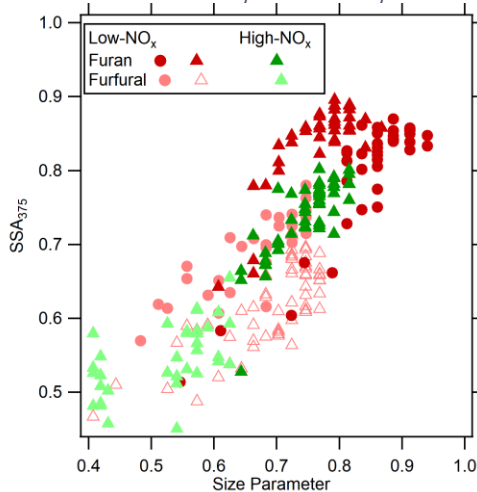

Figure 4: SSA as a function of size parameter for furan and furfural under high/low NO_x non-seeded conditions. Triangle and circular markers of same color represent the duplicate runs of the same condition.

17

3.2 Mass Absorption Coefficient (MAC)

Values of MAC at 375 nm as a function of experiment time for furfural, furan, and thiophene are shown in Figure 4. In all experiments, MAC values were higher in the beginning and then decreased as oxidation progressed. In the later stages of the experiments, furfural showed the highest MAC value of ~ 0.4-0.5 m^2 g^{-1} with furan SOA coming next with MAC values of ~ 0.2-0.3 m^2 g^{-1} and thiophene SOA showed the lowest MAC of ~ 0.1 m^2 g^{-1} (averaged) in the low-NO$_x$, non-seeded conditions. MAC values for furfural and furan SOA in the high-NO$_x$, non-seeded conditions were ~ 0.4-0.6 and ~ 0.15-0.3 m^2 g^{-1}, respectively. MAC values observed in our high-NO$_x$ conditions are not significantly lower than those observed in low-NO$_x$ conditions at longer oxidation times considering the uncertainty of 22% in our MAC calculations. However, there appears to be a significant difference in MAC in early stages of oxidation of furfural, with lower values observed during the high-NO$_x$ conditions, suggesting the role of NO$_x$ in driving the formation of absorbing SOA in the beginning of the experiments. During the seeded experiments for both furfural and furan, lower MAC values of ~ 0.2-0.3 and ~ 0.1-0.2 m^2 g^{-1} were observed, respectively, suggesting formation of non-chromophoric SOA components in the presence of seed. In fact, absorption coefficients at 375 nm during seeded and non-seeded furan and furfural experiments were relatively similar, while a factor of two higher organic mass was formed during the seeded experiments, resulting in lower overall MAC values.
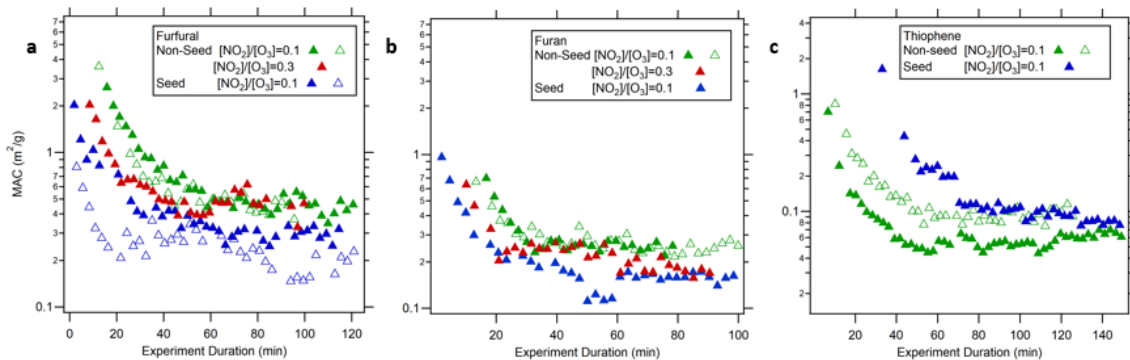
18

Figure 5: MAC vs experiment duration of a) Furfural-derived SOA b) Furan-derived SOA c) Thiophene-derived SOA under non-seeded low-NOx (green markers), seeded low-NOx (blue markers), and non-seeded high-NOx (red markers) experimental conditions. Open and closed markers represent the duplicate runs of the same condition.

A parallel comparison of volume and mass distributions of pyrrole and 1-methylpyrrole SOA in order to calculate their ρ_{eff} have shown a larger d_m compared to d_{va} (Figure 6a), suggesting formation of non-spherical particles during the seeded and non-seeded experiments. To investigate the shape of the SOA particles formed in these experiments, TEM samples were collected during a non-seeded pyrrole experiment. The TEM image (Figure 6b) clearly shows presence of agglomerates of individual spherical SOA on the grid. Since the assumption of particle sphericity is needed for MAC calculation and RI retrievals (through applying Mie theory), we only investigated the chemical evolution of these experiments based on our AMS data.
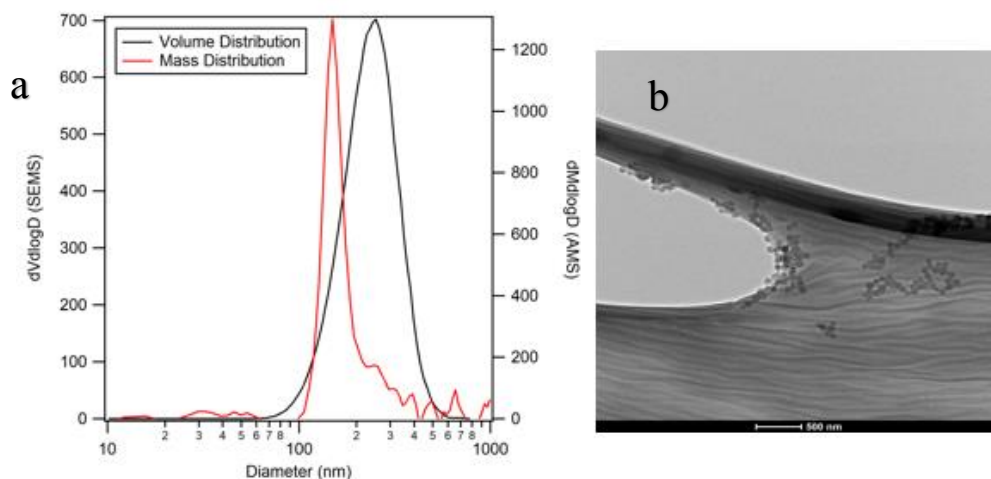
Figure 6:Pyrrole SOA under low-NO$_x$ condition a) volume (SEMS) and mass distribution (AMS) comparison b) TEM images of pyrrole SOA particles

Also, a parallel comparison of volume and mass distributions of thiophene non-seeded experiment (ρ_{eff} close to 1) suggest that thiophene SOA particles are likely to be non-spherical (Figure 7). Thus, our calculations for MAC for thiophene SOAs are susceptible to more uncertainties.

Figure 7: Non-seeded thiophene SOA volume (from SEMS) and Mass (from AMS) distribution under low-NO$_x$ condition

20

3.3 Imaginary Component of RI

Figure 8 represents the imaginary components of RI at 375 nm. Similar to MAC, k values were higher in the beginning of each experiment and decreased with oxidation. Higher k values for furfural ~0.04-0.02 (decreasing trend) compared to furan are consistent with its MAC values also being higher.

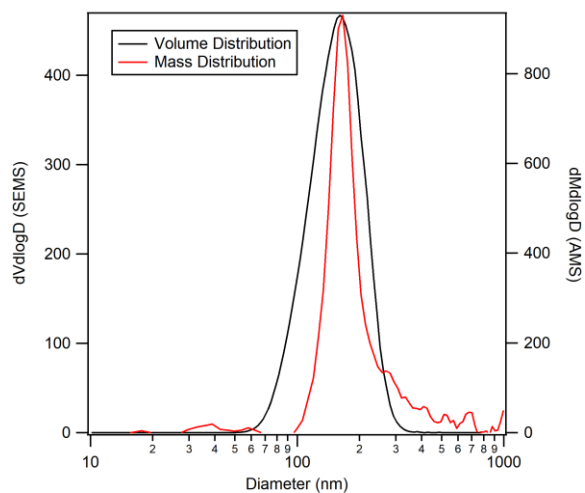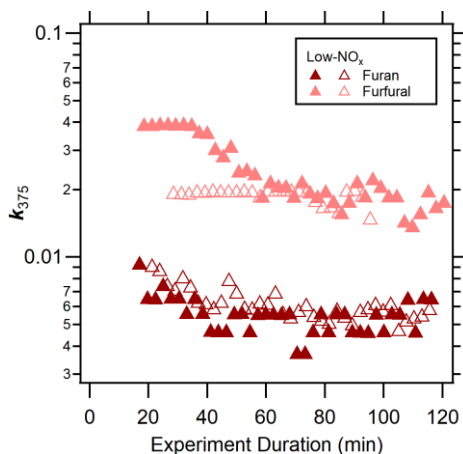*Figure 8: k_{org} at 375 nm retrieved for SOA from oxidation of furan and furfural at different NOx levels*

3.4 Bulk Composition of SOA

To better understand the chemical evolution of SOA in different experiments that drive the differences in optical properties, high-resolution (HR) analyses of mAMS spectra were carried out.

3.3.1 HR Families

The evolution of the contribution of different HR families to the total SOA mass concentration as a function of time is shown in Figures 9-13. For both furan and furfural SOA, $C_xH_xO^+$ components made up the highest fraction of total SOA mass with significant intensities at m/z=29 (CHO^+), indicative of a carbonyl functional group. Another intense signal was observed at m/z=44 (CO_2^+), which is a signature of organic acids. $C_xH_xO_z^+$ (z>1)

components showed a slightly increasing trend throughout the experiments and under different conditions, confirming additional formation of higher oxygenated products as experiments progressed. During the furfural seeded experiment, higher contributions of $C_xH_xO_z^+$ were observed contrary to the expectation, suggesting more oxygenated products were condensed onto seed particles compared to the nucleation experiments. Also, in furfural high-NO_x experiments, a higher contribution of $C_xH_yON^+$ species was observed with significant signals at m/z=86 ($C_3H_6N_2O^+$), m/z=100 ($C_5H_{10}NO^+$), m/z=55 (C_2HNO^+), and m/z=54 (C_2NO^+). This trend is similar to trends observed for furan experiments during high and low NO_x conditions. However, during low-NO_x seeded and non-seeded conditions for furfural, $C_xH_yN^+$ contributions to total SOA mass is higher than $C_xH_yON^+$ species. NO_x levels in furan experiments showed no effect on the generation of more or less nitrogen-containing species. It is important to note that furfural-derived SOA mass concentration in low-NO_x seeded and non-seeded conditions were higher than high-NO_x conditions, indicating the presence of more volatile oxidation products that did not condense onto aerosols when the NO_x level was higher. SOA mass concentration for furan in all different conditions were relatively similar.
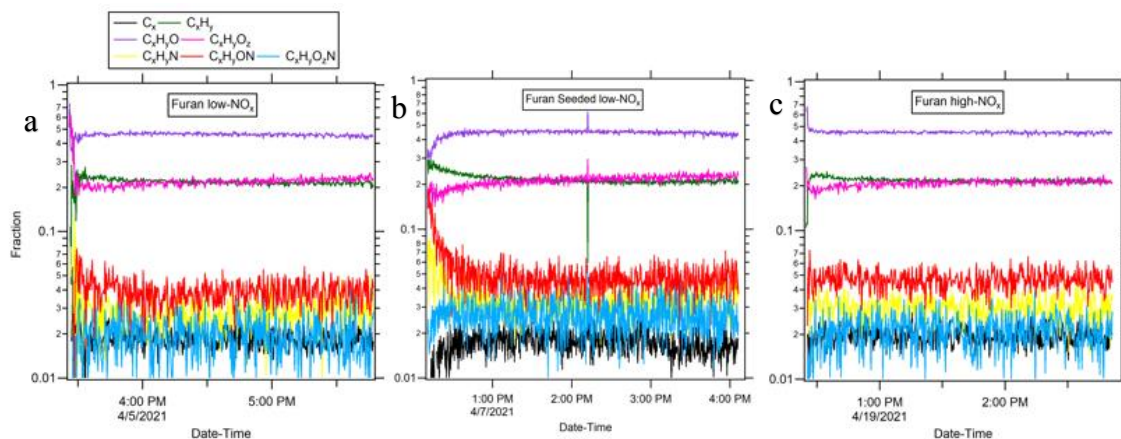
Figure 9: Time evolution of C_x^+ (black), $C_xH_y^+$ (green), $C_xH_yO^+$ (purple), $C_xH_yO_z^+$ (pink), $C_xH_yN^+$ (yellow), CxH_yON^+ (red), and $CxH_yO_zN^+$ (blue) ion families for Furan-derived SOA under (a) Low-NOx, non-seeded, (b) Low-NOx, seeded, and (c) High-NOx, non-seeded conditions.

Figure 10: Time evolution of C_x^+, $C_xH_y^+$, $C_xH_yO^+$, $C_xH_yO_z^+$, $C_xH_yN^+$, CxH_yON^+, and $CxH_yO_zN^+$ ion families for Furfural-derived SOA under (a) Low-NOx, non-seeded, (b) Low-NOx, seeded, and (c) High-NOx, non-seeded conditions.

Similar to furan and furfural experiments, $C_xH_yO^+$ species contributed to the largest fraction of thiophene-derived SOA mass. SOA mass concentration for thiophene was higher during seeded experiments with an increasing trend in the contribution of $C_xH_yO_z^+$ compounds. Also, slightly increased trend in the contributions of $C_xH_yO_zN^+$ and $C_xH_yON^+$ species with respect to time can be indicative of higher condensation of nitrogen-containing compounds during seeded and non-seeded experiments of thiophene.
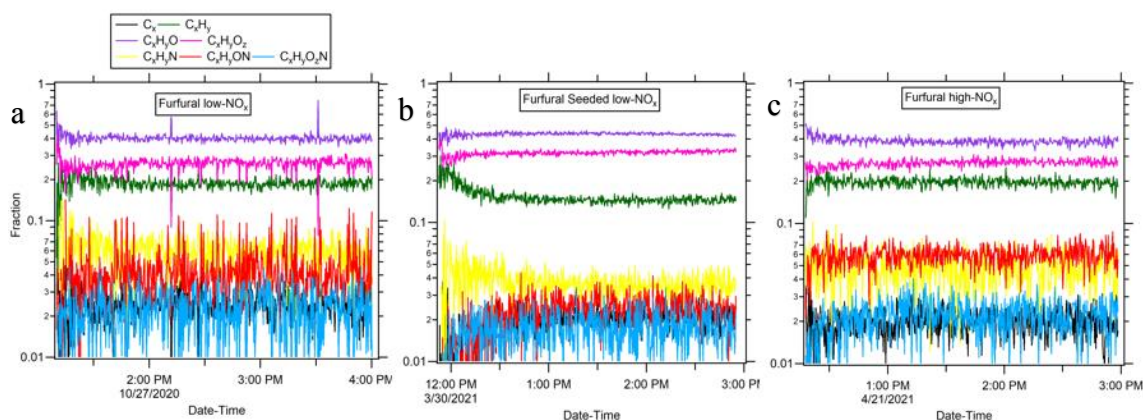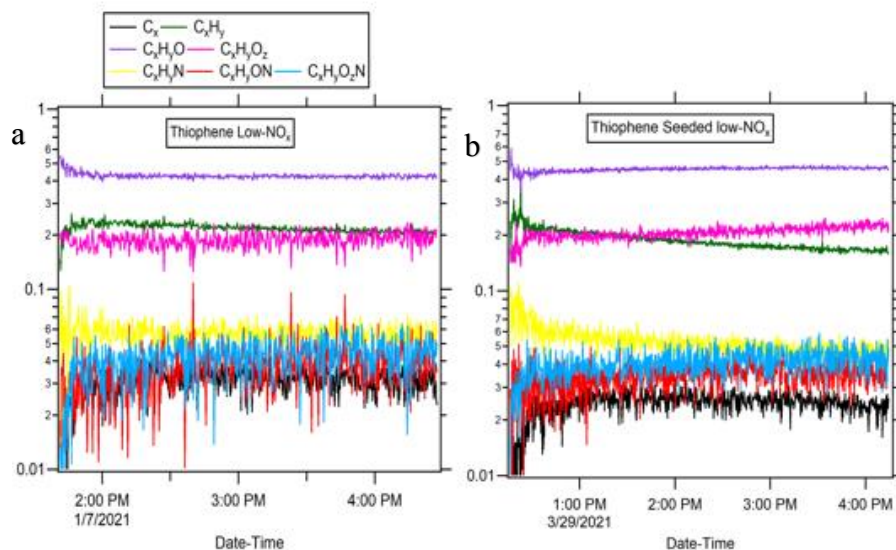
23

Figure 11: Time evolution of $C_x{}^+$, $C_xH_y{}^+$, $C_xH_yO^+$, $C_xH_yO_z{}^+$, $C_xH_yN^+$, $CxHyON^+$, and $CxHyO_zN^+$ ion families for Thiophene-derived SOA under (a) Low-NOx, non-seeded, (b) Low-NOx, seeded.

Pyrrole and 1-methylpyrrole SOA furmed in low-NO_x seeded and non-seeded experiments showed a similar trend for different species. $C_xH_yN^+$ and $C_xH_yO^+$ species comprised the highest fractions with significant signals at m/z=27 (CHN^+) while C_x and $C_xH_yO_zN^+$ (z>1) compounds for both precursors contributed to the lowest fractions of the total SOA mass. Both seeded and non-seeded 1-methylpyrrole experiments exhibit significant intensities at m/z=42 ($C_2H_4N^+$) and m/z=41 ($C_2H_3N^+$) which were not observed in pyrrole experiments. Increasing trends in the contribution of $C_xH_yON^+$ and $C_xH_yO_z{}^+$ species was observed for both precursors, indicating condensation of oxygenated species with experimental time.

Overall, for all five precursors in this study, the most notable change is for $C_xH_yON^+$ and $C_xH_yN^+$ species which was higher in pyrrole and 1-methylpyrrole due to the molecular structure of both parent VOCs containing nitrogen. For all of the other VOCs, presence of these ion families is due to formation of organonitrate/nitroorganics.

24

It is important to note that by comparing trends in HR families and MAC time series in early stages of all the experiments, a decreasing trend in $C_xH_yN^+$ family is observed which can be linked to the observed decreasing trend in the MAC in each experiment, suggesting that this family is likely the contributing chromophore in SOA particles in each experiment.

Figure 12: Time evolution of C_x^+, $C_xH_y^+$, $C_xH_yO^+$, $C_xH_yO_z^+$, $C_xH_yN^+$, $CxHyON^+$, and $CxHyO_zN^+$ ion families for pyrrole-derived SOA under (a) Low-NOx, non-seeded, (b) Low-NOx, seeded.
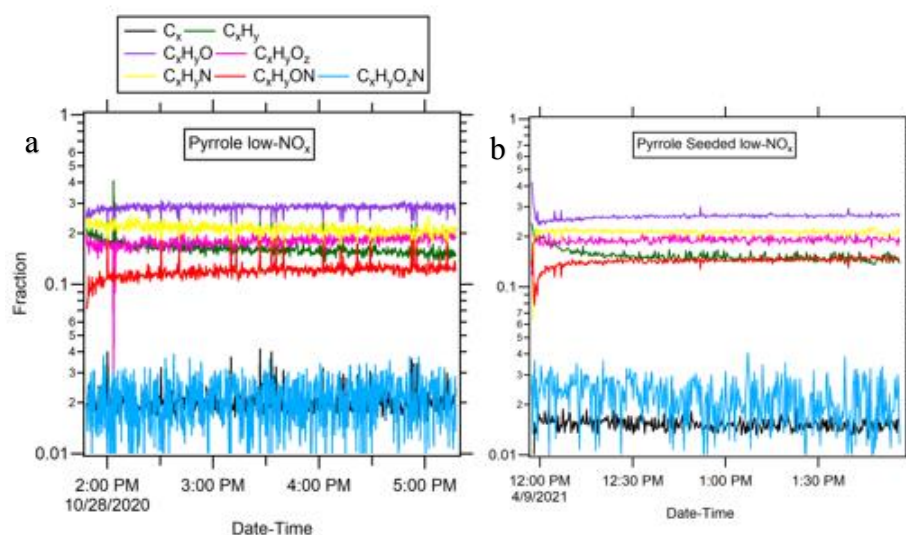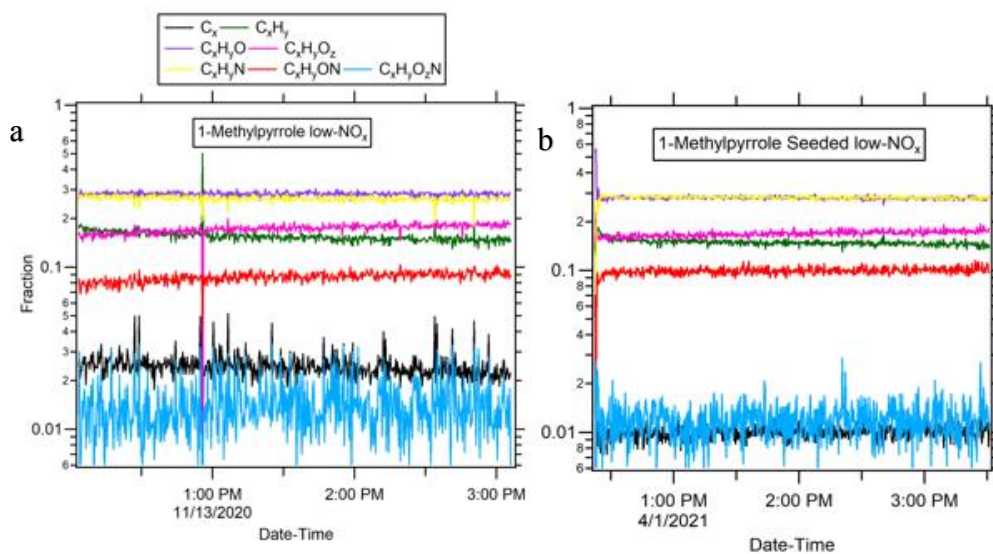

Figure 13: Time evolution of C_x^+, $C_xH_y^+$, $C_xH_yO^+$, $C_xH_yO_z^+$, $C_xH_yN^+$, $CxHyON^+$, and $CxHyO_zN^+$ ion families for 1-methylpyrrole-derived SOA under (a) Low-NOx, non-seeded, (b) Low-NOx, seeded.

25

Previously, Lambe et al. observed that MAC values and imaginary component of refractive indices of SOA increased with increasing oxidation level and decreased with increasing wavelength.[49] In our studies, to estimate SOA oxidation level to then evaluate its correlation with the observed MAC values, we explored the evolution of oxygenated organic aerosols (OOA) through investigating the contribution of the organic aerosol ion signal intensity at m/z=44 (CO$_2^+$) normalized to the total signal intensity of SOA (f44) during the experiment.[13,53] Previous studies have shown that more oxidized components, referred to as low-volatility OOA (LV-OOA), are characterized with higher f44 while less oxidized components, referred to as semi-volatile OOA (SV-OOA), have lower f44.[12,13,53] Evolution of the mass fraction of CO$_2^+$ is shown in Figure 14. Both furfural and furan showed similar f44 during the non-seeded, low-NO$_x$ experiments, suggesting a similar degree of oxidation of organic aerosols due to the similarity of the parent molecules (Figure 14a). In high-NO$_x$ experiments (Figure 14b), contrary to the low-NO$_x$ observations, f44 decreased with SOA oxidation time from ~0.3 to ~0.23 and from ~0.3 to 0.2 for furan and furfural SOA, respectively. Under the low-NO$_x$ condition, thiophene showed the lowest f44 suggesting a significantly lower oxidation degree of SOA during non-seeded, low-NO$_x$ conditions. During seeded experiments, thiophene-derived SOA show higher f44, thus higher oxidation products formation compared to the non-seeded conditions. In contrast, seeded experiments led to lower f44 or lower LV-OOA products for furan while presence of seed did not affect the oxidation degree of products in furfural experiments.
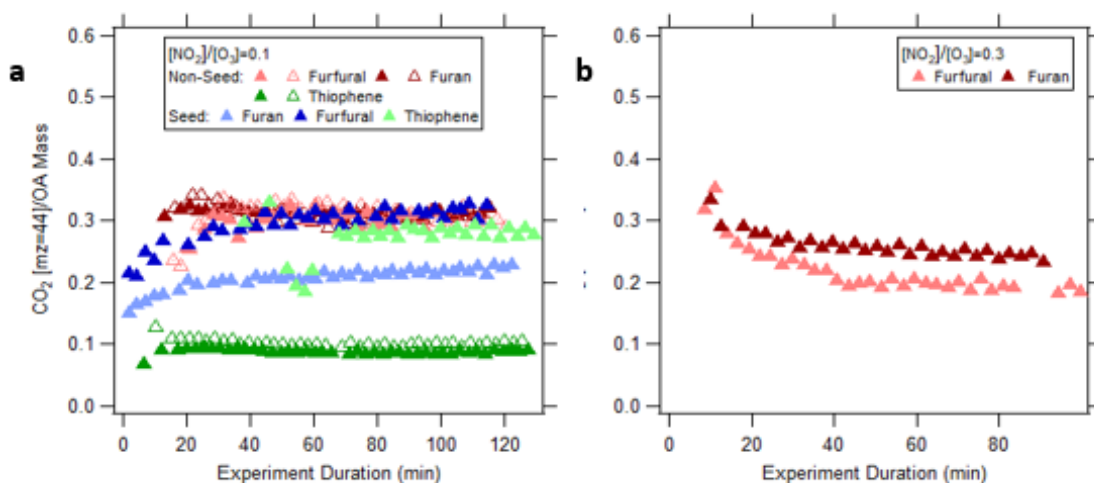
Figure 14: Time series of mass fraction of CO2+ [m/z=44] a) for seeded and non-Seeded systems at low-NOx b) non-seeded at high-NOx

3.3.3 Organonitrate Fraction Time Series

As discussed in previous section, $[NO^+]/[NO_2^+]$ is higher for organic nitrates or nitroorganics than inorganic nitrates. For all experiments the R_{ON} was either 3.57 or 3.9, which is higher than the R_{AN} obtained from atomizing pure ammonium nitrate into our AMS (1.36 ± 0.07). The ratio of organonitrate/nitroorganics ions to measured organics (f_{ON}) for all experiments is calculated from $x\frac{[NO_3^-]}{[OA]}$ and is shown in Figure 15. The calculated f_{ON} slightly increased at the beginning and started to decrease as oxidation progressed under non-seeded low-NOx conditions for all three precursors. The decreasing trend for non-seeded low-NOx and high-NOx is similar to the trend observed in the corresponding SOA's MAC values, suggesting that with decreased organonitrate/nitroorganic formation as SOA were being oxidized, less light-absorbing components were present in the aerosol phase. The calculated f_{ON} for furfural under non-seeded low-NOx condition was higher compared

27

to seeded or high-NO_x conditions, indicating that the presence of NO_x or seed did not increase the formation of organonitrates and/or nitroorganics for furfural SOA. Higher f_{ON} values for furfural in the latter stages of the experiments under low-NO_x conditions compared to high-NO_x is not consistent with the corresponding MAC values if organonitrate/nitroorganics were the dominant chromophores in this system; therefore, additional experiments need to be performed for a more definitive conclusion. An increasing trend was observed for f_{ON} for furfural and furan seeded experiments. Along with the increasing trend of f_{44}, this suggests higher contribution of both oxygen-containing and nitrogen-containing products on seed aerosols as experiments progressed. The overall low MAC values in seeded experiments are consistent with the low f_{ON} values observed for these experiments. Furan SOA formed under high-NO_x condition showed higher f_{ON} values while MAC was actually lower in these conditions. Therefore, more experiments need to be conducted to fully understand the relationship between f_{ON} and MAC values. Thiophene seeded experiments showed higher f_{ON} compared to non-seeded which is in accordance with the observed higher MAC values in the seeded experiments. Lower f_{44} and f_{ON} observed for thiophene non-seeded experiments suggest lower condensation of organonitrate/nitroorganics and oxygenated products into aerosol phase. However, seed particles in thiophene experiments have led to enhanced partitioning of light-absorbing compounds compare to non-seeded experiments. Overall, it is likely that there is a correlation between calculated f_{ON} and the observed MAC values, suggesting that lower contribution of organonitrate/nitroorganics can lead to lowered MAC in these systems. Additional experiments will improve confidence in these results.
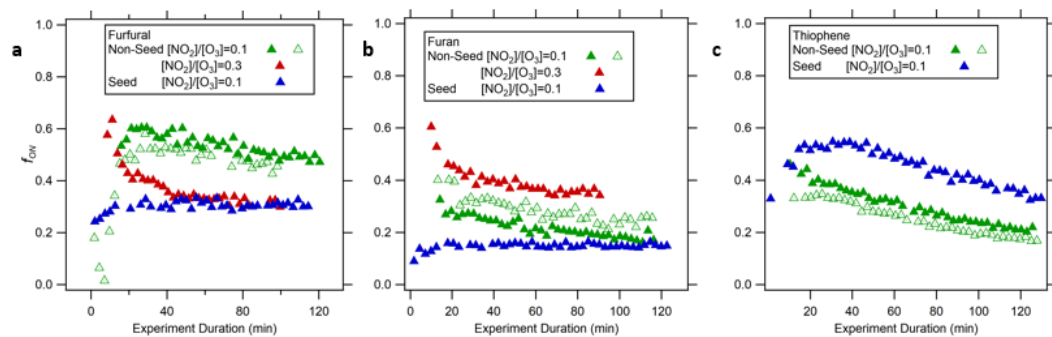
Figure 15: Calculated R_{ON} of a) furfural b) furan c) thiophene as function of experiment duration under low-NOx seeded/non-seeded and high-NOx conditions

3.3.4 Organosulfur Compounds in Thiophene

There is an increasing evidence that organosulfates (OS) in SOA contribute to light absorption.[54–56] However, high level of uncertainty remains in the identification and quantification of OS. Figure 16 shows the time series of SO_x^+ (SO_2^+, SO_3^+, HSO_3^+, and $H_2SO_4^+$) ions ratios over SO^+ ion for thiophene and pure AS. As discussed previously, smaller ions like SO^+, SO_2^+, and SO_3^+ are the dominant fragments during OS fragmentation. With oxidation of thiophene, SO_3^+, HSO_3^+, and $H_2SO_4^+$ ratios increased suggesting formation of oxidized sulfur and/or inorganic sulfates as oxidation progressed. It is important to note that the fraction of $C_xH_ySO_z^+$ (dominated by CHS^+ and $C_2H_2S^+$) over the total OA mass also increased with oxidation, accounting for ~14% and ~23% of the total OA mass at the peak for non-seeded and seeded experiments, respectively (Figure 17). Detection of organosulfur fragments in mAMS was consistent with results from Filter Inlet for GAses and AEROsols coupled to a chemical ionization high-resolution time-of-flight mass spectrometer (FIGAERO-CIMS) which also showed trace amounts of organosulfur compounds present in the aerosol phase (e.g., $C_4H_3NO_4S$ and $C_4H_5NO_7S$).

However, in both of these observations, source of sulfur is likely thiophene itself, but more investigation on the structure of these compounds is needed to differentiate between organosulfur vs. OS species.
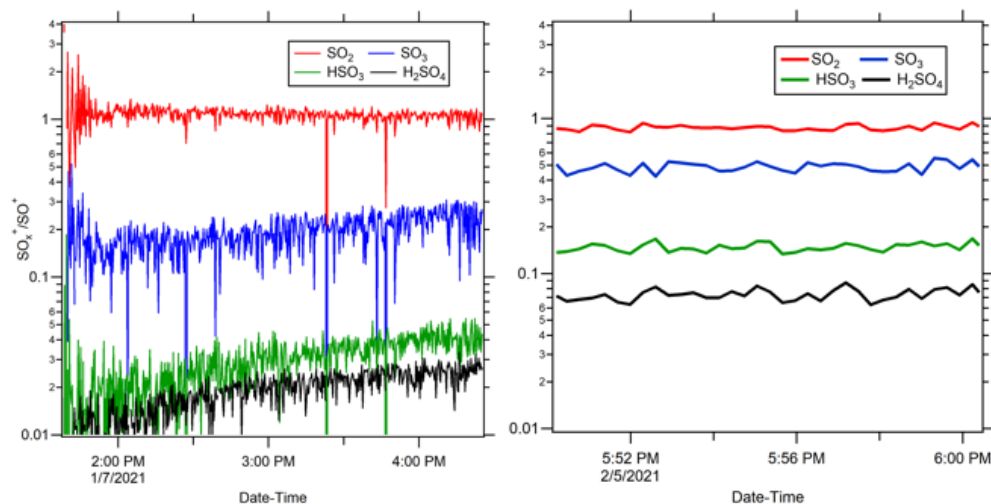

Figure 16: Comparison of SO_x^+/SO^+ ratios in a) thiophene and b) pure ammonium sulfate (AS)
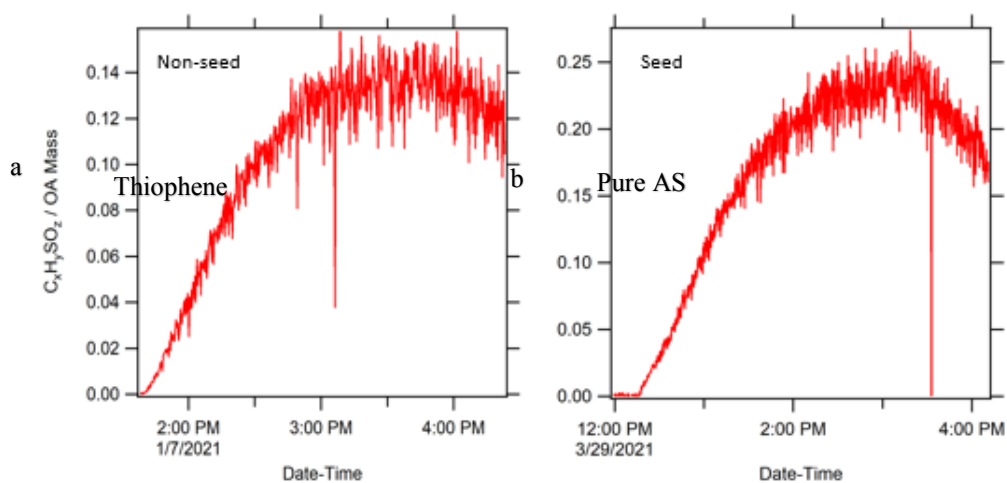

Figure 17: fractional Contributions of CS Family to OA Mass in seeded and non-seeded thiophene experiments

CHAPTER IV: CONCLUSIONS

In this study, we observed different optical properties and chemical compositions for the SOA formed from oxidation of unsaturated heterocyclic compounds in the presence of NO_3 radicals in the dark. Our analysis reveals that organonitrates/nitroorganics are formed, potentially leading to the formation of light-absorbing secondary BrC. Among all the precursors and at large size parameters, pyrrole- derived SOA formed under low NO_x, non- seeded conditions showed the lowest SSA while 1-methylpyrrole and thiophene showed the highest. Furfural and furan had intermediate SSA values. The difference in SSA for pyrrole and 1-methylpyrrole can be due to the presence of the methyl group which can make 1-methylpyrrole undergoing different chemistry when reacting with NO_3 radicals. Among furfural, furan, and thiophene, furfural-derived BrC generated in low and high NO_x seeded and non-seeded conditions showed the highest MAC and k values, confirming the formation of more light-absorbing compounds. Due to the non-spherical shape of the particles formed from pyrrole and 1-methylpyrrole, we could not evaluate their MAC and k parameters. In high-NO_x condition, furan SOA showed higher k that confirms a higher contribution of or presence of more light-absorbing species within the aerosols. Both furan and furfural SOA formed in seeded experiments had lower MAC compared to the non-seeded experiments, which suggests a relatively lower contribution of BrC species to SOA in the presence of seed particles. Thiophene seeded experiments on the other hand showed higher MAC especially in the early stages of the experiments, likely due to higher contributions from organonitrates/nitroorganics and organosulfur compounds.

REFERENCES

1.   Yan J, Wang X, Gong P, Wang C, Cong Z. Review of brown carbon aerosols: Recent progress and perspectives. *Sci Total Environ*. 2018;634:1475-1485. doi:https://doi.org/10.1016/j.scitotenv.2018.04.083

2.   Di Lorenzo RA, Young CJ. Size separation method for absorption characterization in brown carbon: Application to an aged biomass burning sample. *Geophys Res Lett*. 2016;43(1):458-465. doi:https://doi.org/10.1002/2015GL066954

3.   Kasthuriarachchi NY, Rivellini L-H, Adam MG, Lee AKY. Light Absorbing Properties of Primary and Secondary Brown Carbon in a Tropical Urban Environment. *Environ Sci Technol*. 2020;54(17):10808-10819. doi:10.1021/acs.est.0c02414

4.   Lin P, Aiona PK, Li Y, et al. Molecular Characterization of Brown Carbon in Biomass Burning Aerosol Particles. *Environ Sci Technol*. 2016;50(21):11815-11824. doi:10.1021/acs.est.6b03024

5.   Jiang H, Frie AL, Lavi A, et al. Brown Carbon Formation from Nighttime Chemistry of Unsaturated Heterocyclic Volatile Organic Compounds. *Environ Sci Technol Lett*. 2019;6(3):184-190. doi:10.1021/acs.estlett.9b00017

6.   Decker ZCJ, Zarzana KJ, Coggon M, et al. Nighttime Chemical Transformation in Biomass Burning Plumes: A Box Model Analysis Initialized with Aircraft Observations. *Environ Sci Technol*. 2019;53(5):2529-2538. doi:10.1021/acs.est.8b05359

7.   Intergovernmental Panel on Climate Change, ed. Anthropogenic and Natural Radiative Forcing. In: *Climate Change 2013 – The Physical Science Basis: Working Group I Contribution to the Fifth Assessment Report of the Intergovernmental Panel on Climate Change*. Cambridge University Press; 2014:659-740. doi:DOI: 10.1017/CBO9781107415324.018

8.   Hallquist M, Wenger JC, Baltensperger U, et al. The formation, properties and impact of secondary organic aerosol: current and emerging issues. *Atmos Chem Phys*. 2009;9(14):5155-5236. doi:10.5194/acp-9-5155-2009

9.   Moise T, Flores JM, Rudich Y. Optical Properties of Secondary Organic Aerosols and Their Changes by Chemical Processes. *Chem Rev*. 2015;115(10):4400-4439. doi:10.1021/cr5005259

10.   Pope CA, Dockery DW. Health Effects of Fine Particulate Air Pollution: Lines that Connect. *J Air Waste Manage Assoc*. 2006;56(6):709-742. doi:10.1080/10473289.2006.10464485

11.   VALAVANIDIS A, FIOTAKIS K, VLACHOGIANNI T. Airborne Particulate Matter and Human Health: Toxicological Assessment and Importance of Size and Composition of Particles for Oxidative Damage and Carcinogenic Mechanisms. *J Environ Sci Heal Part C*. 2008;26(4):339-362. doi:10.1080/10590500802494538

12.   Jimenez JL, Canagaratna MR, Donahue NM, et al. Evolution of Organic Aerosols in the Atmosphere. *Science (80-)*. 2009;326(5959):1525 LP - 1529. doi:10.1126/science.1180353

13.   Ng NL, Canagaratna MR, Zhang Q, et al. Organic aerosol components observed in Northern Hemispheric datasets from Aerosol Mass Spectrometry. *Atmos Chem Phys*. 2010;10(10):4625-4641. doi:10.5194/acp-10-4625-2010

14.   Kanakidou M, Seinfeld JH, Pandis SN, et al. Organic aerosol and global climate modelling: a review. *Atmos Chem Phys*. 2005;5(4):1053-1123. doi:10.5194/acp-5-1053-2005

15.   Bond TC, Bergstrom RW. Light Absorption by Carbonaceous Particles: An Investigative Review. *Aerosol Sci Technol*. 2006;40(1):27-67. doi:10.1080/02786820500421521

16.   Lee HJ (Julie), Aiona PK, Laskin A, Laskin J, Nizkorodov SA. Effect of Solar Radiation on the Optical Properties and Molecular Composition of Laboratory Proxies of Atmospheric Brown Carbon. *Environ Sci Technol*. 2014;48(17):10217-10226. doi:10.1021/es502515r

17.   Andreae MO, Gelencsér A. Black carbon or brown carbon? The nature of light-absorbing carbonaceous aerosols. *Atmos Chem Phys*. 2006;6(10):3131-3148. doi:10.5194/acp-6-3131-2006

18.   Laskin A, Laskin J, Nizkorodov SA. Chemistry of Atmospheric Brown Carbon. *Chem Rev*. 2015;115(10):4335-4382. doi:10.1021/cr5006167

19.   Lewis K, Arnott WP, Moosmüller H, Wold CE. Strong spectral variation of biomass smoke light absorption and single scattering albedo observed with a novel dual-wavelength photoacoustic instrument. *J Geophys Res Atmos*. 2008;113(D16). doi:https://doi.org/10.1029/2007JD009699

20.   Zhang X, Lin Y-H, Surratt JD, Weber RJ. Sources, Composition and Absorption Ångström Exponent of Light-absorbing Organic Components in Aerosol Extracts

from the Los Angeles Basin. *Environ Sci Technol*. 2013;47(8):3685-3693. doi:10.1021/es305047b

21.   Feng Y, Ramanathan V, Kotamarthi VR. Brown carbon: a significant atmospheric absorber of solar radiation? *Atmos Chem Phys*. 2013;13(17):8607-8621. doi:10.5194/acp-13-8607-2013

22.   Mohr C, Lopez-Hilfiker FD, Zotter P, et al. Contribution of Nitrated Phenols to Wood Burning Brown Carbon Light Absorption in Detling, United Kingdom during Winter Time. *Environ Sci Technol*. 2013;47(12):6316-6324. doi:10.1021/es400683v

23.   Powelson MH, Espelien BM, Hawkins LN, Galloway MM, De Haan DO. Brown Carbon Formation by Aqueous-Phase Carbonyl Compound Reactions with Amines and Ammonium Sulfate. *Environ Sci Technol*. 2014;48(2):985-993. doi:10.1021/es4038325

24.   Grace DN, Sharp JR, Holappa RE, et al. Heterocyclic Product Formation in Aqueous Brown Carbon Systems. *ACS Earth Sp Chem*. 2019;3(11):2472-2481. doi:10.1021/acsearthspacechem.9b00235

25.   Takemura T, Nakajima T, Dubovik O, Holben BN, Kinne S. Single-Scattering Albedo and Radiative Forcing of Various Aerosol Species with a Global Three-Dimensional Model. *J Clim*. 2002;15(4):333-352. doi:10.1175/1520-0442(2002)015<0333:SSAARF>2.0.CO;2

26.   Srinivas B, Rastogi N, Sarin MM, Singh A, Singh D. Mass absorption efficiency of light absorbing organic aerosols from source region of paddy-residue burning emissions in the Indo-Gangetic Plain. *Atmos Environ*. 2016;125:360-370. doi:https://doi.org/10.1016/j.atmosenv.2015.07.017

27.   Dingle JH, Zimmerman S, Frie AL, Min J, Jung H, Bahreini R. Complex refractive index, single scattering albedo, and mass absorption coefficient of secondary organic aerosols generated from oxidation of biogenic and anthropogenic precursors. *Aerosol Sci Technol*. 2019;53(4):449-463. doi:10.1080/02786826.2019.1571680

28.   Reid JS, Koppmann R, Eck TF, Eleuterio DP. A review of biomass burning emissions part II: intensive physical properties of biomass burning particles. *Atmos Chem Phys*. 2005;5(3):799-825. doi:10.5194/acp-5-799-2005

29.   Hatch LE, Luo W, Pankow JF, Yokelson RJ, Stockwell CE, Barsanti KC. Identification and quantification of gaseous organic compounds emitted from biomass burning using two-dimensional gas chromatography–time-of-flight mass

spectrometry. *Atmos Chem Phys*. 2015;15(4):1865-1899. doi:10.5194/acp-15-1865-2015

30. Kelly JM, Doherty RM, O'Connor FM, Mann GW. The impact of biogenic, anthropogenic, and biomass burning volatile organic compound emissions on regional and seasonal variations in secondary organic aerosol. *Atmos Chem Phys*. 2018;18(10):7393-7422. doi:10.5194/acp-18-7393-2018

31. Li C, He Q, Fang Z, et al. Laboratory Insights into the Diel Cycle of Optical and Chemical Transformations of Biomass Burning Brown Carbon Aerosols. *Environ Sci Technol*. 2020;54(19):11827-11837. doi:10.1021/acs.est.0c04310

32. Jo DS, Park RJ, Lee S, Kim S-W, Zhang X. A global simulation of brown carbon: implications for photochemistry and direct radiative effect. *Atmos Chem Phys*. 2016;16(5):3413-3432. doi:10.5194/acp-16-3413-2016

33. Brown H, Liu X, Feng Y, et al. Radiative effect and climate impacts of brown carbon with the Community Atmosphere Model (CAM5). *Atmos Chem Phys*. 2018;18(24):17745-17768. doi:10.5194/acp-18-17745-2018

34. Lin P, Bluvshtein N, Rudich Y, Nizkorodov SA, Laskin J, Laskin A. Molecular Chemistry of Atmospheric Brown Carbon Inferred from a Nationwide Biomass Burning Event. *Environ Sci Technol*. 2017;51(20):11561-11570. doi:10.1021/acs.est.7b02276

35. Vakkari V, Kerminen V-M, Beukes JP, et al. Rapid changes in biomass burning aerosols by atmospheric oxidation. *Geophys Res Lett*. 2014;41(7):2644-2651. doi:https://doi.org/10.1002/2014GL059396

36. Simpson IJ, Akagi SK, Barletta B, et al. Boreal forest fire emissions in fresh Canadian smoke plumes: C_1-C_{10} volatile organic compounds (VOCs), CO_2, CO, NO_2, NO, HCN and CH_3CN. *Atmos Chem Phys*. 2011;11(13):6445-6463. doi:10.5194/acp-11-6445-2011

37. Li C, He Q, Hettiyadura APS, et al. Formation of Secondary Brown Carbon in Biomass Burning Aerosol Proxies through NO3 Radical Reactions. *Environ Sci Technol*. 2020;54(3):1395-1405. doi:10.1021/acs.est.9b05641

38. Williams AP, Abatzoglou JT, Gershunov A, et al. Observed Impacts of Anthropogenic Climate Change on Wildfire in California. *Earth's Futur*. 2019;7(8):892-910. doi:https://doi.org/10.1029/2019EF001210

39. Doerr SH, Santín C. Global trends in wildfire and its impacts: perceptions versus realities in a changing world. *Philos Trans R Soc B Biol Sci*.

2016;371(1696):20150345. doi:10.1098/rstb.2015.0345

40. Sumlin BJ, Pandey A, Walker MJ, Pattison RS, Williams BJ, Chakrabarty RK. Atmospheric Photooxidation Diminishes Light Absorption by Primary Brown Carbon Aerosol from Biomass Burning. *Environ Sci Technol Lett*. 2017;4(12):540-545. doi:10.1021/acs.estlett.7b00393

41. Forrister H, Liu J, Scheuer E, et al. Evolution of brown carbon in wildfire plumes. *Geophys Res Lett*. 2015;42(11):4623-4630. doi:https://doi.org/10.1002/2015GL063897

42. Selimovic V, Yokelson RJ, McMeeking GR, Coefield S. In situ measurements of trace gases, PM, and aerosol optical properties during the 2017 NW US wildfire smoke event. *Atmos Chem Phys*. 2019;19(6):3905-3926. doi:10.5194/acp-19-3905-2019

43. Cui Y, Frie AL, Dingle JH, et al. Influence of Ammonia and Relative Humidity on the Formation and Composition of Secondary Brown Carbon from Oxidation of 1-Methylnaphthalene and Longifolene. *ACS Earth Sp Chem*. 2021;5(4):858-869. doi:10.1021/acsearthspacechem.0c00353

44. Shen G, Chen Y, Wei S, Fu X, Zhu Y, Tao S. Mass absorption efficiency of elemental carbon for source samples from residential biomass and coal combustions. *Atmos Environ*. 2013;79:79-84. doi:https://doi.org/10.1016/j.atmosenv.2013.05.082

45. Bahreini R, Keywood MD, Ng NL, et al. Measurements of Secondary Organic Aerosol from Oxidation of Cycloalkenes, Terpenes, and m-Xylene Using an Aerodyne Aerosol Mass Spectrometer. *Environ Sci Technol*. 2005;39(15):5674-5688. doi:10.1021/es048061a

46. Farmer DK, Matsunaga A, Docherty KS, et al. Response of an aerosol mass spectrometer to organonitrates and organosulfates and implications for atmospheric chemistry. *Proc Natl Acad Sci*. 2010;107(15):6670-6675. doi:10.1073/pnas.0912340107

47. Fry JL, Draper DC, Zarzana KJ, et al. Observations of gas- and aerosol-phase organic nitrates at BEACHON-RoMBAS 2011. *Atmos Chem Phys*. 2013;13(17):8585-8605. doi:10.5194/acp-13-8585-2013

48. Chen Y, Xu L, Humphry T, et al. Response of the Aerodyne Aerosol Mass Spectrometer to Inorganic Sulfates and Organosulfur Compounds: Applications in Field and Laboratory Measurements. *Environ Sci Technol*. 2019;53(9):5176-5186. doi:10.1021/acs.est.9b00884

49. Lambe AT, Cappa CD, Massoli P, et al. Relationship between Oxidation Level and Optical Properties of Secondary Organic Aerosol. *Environ Sci Technol*. 2013;47(12):6349-6357. doi:10.1021/es401043j

50. Kim H, Barkey B, Paulson SE. Real refractive indices of α- and β-pinene and toluene secondary organic aerosols generated from ozonolysis and photo-oxidation. *J Geophys Res Atmos*. 2010;115(D24). doi:https://doi.org/10.1029/2010JD014549

51. Kim H, Paulson SE. Real refractive indices and volatility of secondary organic aerosol generated from photooxidation and ozonolysis of limonene, α-pinene and toluene. *Atmos Chem Phys*. 2013;13(15):7711-7723. doi:10.5194/acp-13-7711-2013

52. Zhang X, Kim H, Parworth CL, et al. Optical Properties of Wintertime Aerosols from Residential Wood Burning in Fresno, CA: Results from DISCOVER-AQ 2013. *Environ Sci Technol*. 2016;50(4):1681-1690. doi:10.1021/acs.est.5b04134

53. Adler G, Flores JM, Abo Riziq A, Borrmann S, Rudich Y. Chemical, physical, and optical evolution of biomass burning aerosols: a case study. *Atmos Chem Phys*. 2011;11(4):1491-1503. doi:10.5194/acp-11-1491-2011

54. Fleming LT, Ali NN, Blair SL, Roveretto M, George C, Nizkorodov SA. Formation of Light-Absorbing Organosulfates during Evaporation of Secondary Organic Material Extracts in the Presence of Sulfuric Acid. *ACS Earth Sp Chem*. 2019;3(6):947-957. doi:10.1021/acsearthspacechem.9b00036

55. Song C, Gyawali M, Zaveri RA, Shilling JE, Arnott WP. Light absorption by secondary organic aerosol from α-pinene: Effects of oxidants, seed aerosol acidity, and relative humidity. *J Geophys Res Atmos*. 2013;118(20):11,711-741,749. doi:https://doi.org/10.1002/jgrd.50767

56. Nguyen TB, Lee PB, Updyke KM, et al. Formation of nitrogen- and sulfur-containing light-absorbing compounds accelerated by evaporation of water from secondary organic aerosols. *J Geophys Res Atmos*. 2012;117(D1). doi:https://doi.org/10.1029/2011JD016944